Energy Proceedings
Vol 50, 2025
ISSN 2004-2965

Thermal Management Design and Parameter Optimization of Battery Energy Storage System Under High Discharge Rate Scenario#

Guangliang Wang[1], Jing Wang[1], Juan Song[1], Jintao Niu[1], Yuhan Ding[1], Yuxin Luo[1], Jun Zhao[12*]

1 Key Laboratory of Efficient Utilization of Low and Medium Grade Energy (Tianjin University), Tianjin 300350, China

2 National Industry-Education Platform of Energy Storage, Tianjin University, Tianjin 300350, China

(Corresponding Author: zhaojun@tju.edu.cn)

ABSTRACT

The lifetime and performance of battery energy storage system depend on the temperature uniformity between batteries. In order to meet the temperature requirements in high discharge rate scenarios, this study proposes a novel composite cooling system. Based on the battery module, a thermal management system integrating PCM cooling, air cooling and liquid cooling is established. The influence of liquid cooling layout and flow direction on temperature uniformity is discussed. The flow parameters of air cooling and liquid cooling are optimized by orthogonal analysis. The results show that liquid-cooled longitudinal flow has better temperature uniformity than cross flow. When the liquid cooling flow direction is completely countercurrent, the maximum temperature difference is reduced to 4.35 K, and the improvement effect is 12.47%. After further auxiliary air cooling with inlet velocity of 0.4 m/s, the maximum temperature difference is reduced to 4.13 K. In general, this study can provide a new idea for BTM of high-rate discharge scenarios.

Keywords: Battery energy storage system, composite cooling, liquid cooling optimization, orthogonal analysis

NONMENCLATURE

Abbreviations	
BESS	Battery Energy Storage System
BTM	Battery Thermal Management
PCM	Phase Change Material
Symbols	
c_p	specific heat capacity, $J \cdot kg^{-1} \cdot K^{-1}$
f_{PCM}	PCM liquid fraction, %
k	turbulent kinetic energy, $m^2 \cdot s^{-2}$
P_{fan}	fan power consumption, kJ
$q_{V,b}$	battery heat generation, $W \cdot m^{-3}$
T	temperature, K
t	time, s
U	velocity, $m \cdot s^{-1}$
ε	turbulent dissipation rate, $m^2 \cdot s^{-3}$
λ	thermal conductivity, $W \cdot m^{-1} \cdot K^{-1}$
μ	dynamic viscosity, $N \cdot s \cdot m^{-2}$
ρ	density, $kg \cdot m^{-3}$

1. INTRODUCTION

With the increasing energy density of battery energy storage system (BESS), the safety problems caused by thermal runaway of batteries have become increasingly prominent. In the past five years, there have been more than 30 fire and explosion cases of energy storage power stations around the world [1].

In general, the optimal operating temperature of energy storage battery is between 288.15 K and 308.15 K [2]. Further, the temperature uniformity between battery modules can also seriously affect the efficiency and performance of the BESS. The maximum temperature difference between batteries should be less than 5 K [3]. Therefore, it is very important to propose a safe and efficient battery thermal management (BTM) for BESS.

At present, the main methods of BTM include air cooling [4], liquid cooling [5], phase change material (PCM) cooling [6] and heat pipe cooling [7]. Air cooling is widely used in BESS due to its advantages of simple equipment, high safety and low cost. Chen et al. [8] proposed a control strategy based on battery temperature difference. Compared with the single flow, the average temperature difference of optimized system was reduced by more than 67%. Zhang et al. [9] discussed the influence of number and position of spoilers in duct. Compared with the initial scheme, the maximum temperature and maximum temperature difference of optimized system were reduced by 1.86 K and 2.51 K, respectively. However, it also has some defects. The specific heat capacity and thermal conductivity of air are

This is a paper for the 16th International Conference on Applied Energy (ICAE2024), Sep. 1-5, 2024, Niigata, Japan.

very small, which can easily cause the temperature difference between the inlet and outlet of system to be too large, causing uneven temperature. Liquid cooling has a very broad application prospect due to its large specific heat capacity and high heat transfer efficiency. Fan et al. [10] proposed a novel type of dendritic liquid-cooling plate based on construction theory. After optimization, the maximum temperature was decreased from 325.74 K to 312.45 K. The flow pressure drop was decreased from 518.6 Pa to 136.5 Pa. Zuo [11] et al. optimized the structure of liquid-cooling plate. The double S-shaped channel had lower flow resistance and higher heat transfer performance than the single S-shaped channel. The pump power was reduced by 73.88%.

In summary, each cooling method has its own limitations. Previous studies have usually been limited to a single cooling method. In order to make full use of the advantages of air cooling and liquid cooling while reducing their shortcomings, this study proposes a novel type of composite cooling system. Based on the battery module, a thermal management system integrating PCM cooling, air cooling and liquid cooling is established. The influence of liquid cooling layout and flow direction on the temperature uniformity of battery module is discussed. The flow parameters of air cooling and liquid cooling are optimized by orthogonal analysis.

2. NUMERICAL SIMULATIONS

2.1 *Physical model*

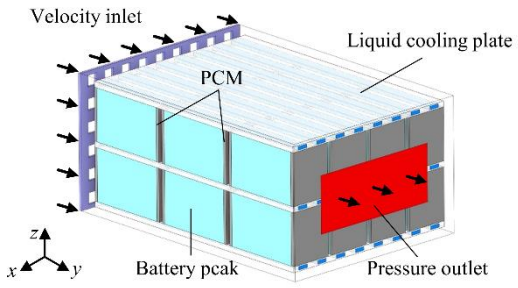

Fig. 1 Physical model.

Fig. 1 shows a novel composite cooling structure. The cooling methods include PCM cooling, air cooling and liquid cooling. The battery module is composed of 24 battery packs in series. The structure size is 544 × 374 × 234 mm. PCM is arranged in the longitudinal small area of battery pack. The thickness of PCM is 6 mm. The melting temperature is 303.15 ~ 305.15 K, and the latent heat of phase change is 150 kJ/kg. The physical parameters of the remaining materials are shown in Table 1. Each battery pack is clamped by two liquid cooling plates to achieve rapid cooling. Air flows through the gap of each battery pack and plays an auxiliary heat dissipation role.

Table 1 Physical parameters of materials in battery module.

Materials	ρ	c_p	λ	μ
Air	1.225	1006.43	0.0242	1.79×10^{-5}
Water	998.2	4182	0.6	1.00×10^{-3}
Battery	2300	1072	1.5, 18.5, 18.5	/
Aluminum plate	2719	871	202.4	/
PCM	1000	2000	1.2	/

2.2 *Mathematical model*

2.2.1 Model assumptions

In order to facilitate battery module modeling and calculation, the following assumptions are made in the study. (1) The heat generation of the battery is considered as the internal heat source. (2) Air is regarded as an incompressible fluid. (3) PCM adopts the equivalent specific heat model. (4) The physical properties of materials do not change with temperature.

2.2.2 Governing equations

The mass, momentum and energy equations in the air and liquid calculation zones are shown in Eqs. 1-3, respectively.

$$\frac{\partial \rho}{\partial t}+\rho\nabla\cdot\vec{U}=0 \tag{1}$$

$$\frac{\partial}{\partial t}\left(\rho\vec{U}\right)+\rho\nabla\cdot\left(\vec{U}\vec{U}\right)=-\nabla p+\mu\nabla\cdot\left(\nabla\vec{U}\right)+\rho\vec{g} \tag{2}$$

$$\rho c_p\left(\frac{\partial T}{\partial t}+\vec{U}\cdot\nabla T\right)=\nabla\cdot\left(\lambda\nabla T\right) \tag{3}$$

In this study, the inlet Reynolds number of battery module is 30789. Therefore, the standard *k-ε* model is chosen to describe the turbulence flow of air, as shown in Eq. 4 and Eq. 5.

$$\frac{\partial}{\partial t}(\rho k)+\frac{\partial}{\partial x_j}(\rho k\mu_j)=\frac{\partial}{\partial x_j}\left(\left(\mu+\frac{\mu_t}{\sigma_k}\right)\frac{\partial k}{\partial x_j}\right)+G_k+G_b-\rho\varepsilon-Y_M \tag{4}$$

$$\frac{\partial}{\partial t}(\rho\varepsilon)+\frac{\partial}{\partial x_j}(\rho\varepsilon\mu_j)=\frac{\partial}{\partial x_j}\left(\left(\mu+\frac{\mu_t}{\sigma_\varepsilon}\right)\frac{\partial\varepsilon}{\partial x_j}\right)+C_{1\varepsilon}\frac{\varepsilon}{k}\left(G_k+C_{3\varepsilon}+G_b\right)-\rho C_{2\varepsilon}\frac{\varepsilon^2}{k} \tag{5}$$

Laminar model is selected for the liquid flow, since the inlet Reynolds number is 460. The equivalent heat capacity method is used to analyze PCM model. The heat transfer differential equation in PCM zones is as follows.

$$\rho_{\mathrm{PCM}}c_{p,\mathrm{PCM}}\frac{\partial T}{\partial t}=\nabla\cdot\left(\lambda_{\mathrm{PCM}}\nabla T_{\mathrm{PCM}}\right)+\rho_{\mathrm{PCM}}L_{\mathrm{PCM}}\frac{\partial f_{\mathrm{PCM}}}{\partial t} \tag{6}$$

The energy equation of battery calculation zones is expressed as follows.

$$\frac{\partial}{\partial t}\left(\rho_{\mathrm{b}}c_{p,\mathrm{b}}T\right)=\nabla\cdot\left(\lambda_{\mathrm{b}}\nabla T\right)+q_{V,\mathrm{b}} \tag{7}$$

As shown in Eq. 7, there is a source term q_V in the energy equation of batteries. Xin et al. [12] tested the heat generation rate of battery by calibration calorimetry

method based on heat transfer theory and energy conservation law, as shown in Eq. 8.

$$q_{V,b} = 26408.12838 - 32.29395t + 0.02572t^2 - 8.77507\times10^{-6}t^3 + 1.15957\times10^{-9}t^4 \quad (8)$$

2.3 *Initial and boundary conditions*

In this study, the ambient temperature is set to 298.15 K. The initial temperature is consistent with the ambient temperature. The velocity inlet and pressure outlet are set as the boundary conditions. The air velocity of inlet is 1.57 m/s. The liquid cooling inlet mass flow rate is 10 L/min.

2.4 *Model validation*

2.4.1. Grid independence

Table 2 shows the comparison results of the maximum temperature and maximum temperature difference of battery module under different grid numbers. When the number of grids is greater than 52864, the error of the maximum temperature and maximum temperature difference caused by continuing to increase the number of grids is less than 0.01 K. Therefore, in order to save the calculation time, this study finally divides calculation model into 52864 grids.

Table 2 Grid independence.

Number	19778	29539	42591	52864	65419	95128
T_{max} K	305.52	306.82	306.78	306.72	306.72	306.71
ΔT_{max} K	2.51	2.61	2.63	2.64	2.64	2.64

2.4.2. Battery heat generation model

In order to verify the accuracy of the numerical results, this study chooses the experiment of Xin et al. for comparison. The results of comparison between this study and experiment are shown in Fig. 2. It can be seen that the numerical results are consistent with the experimental results.

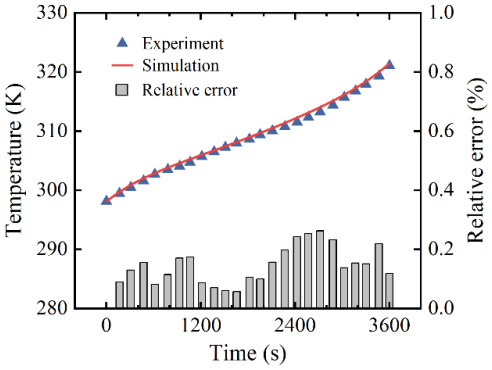

Fig. 2. Comparison of simulation and experiment.

3. RESULTS AND DISCUSSION

3.1 *Effect of liquid cooling layout*

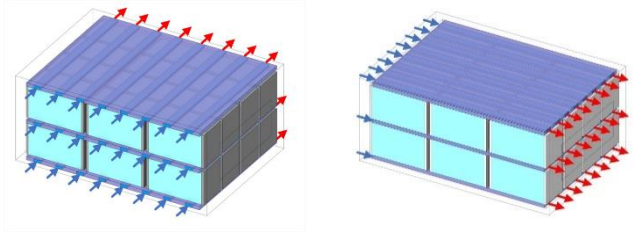

(a) *(b)*

Fig. 3. Liquid cooling layout. (a) Cross flow; (b) Longitudinal flow.

In this study, the effect of two liquid cooling layouts, cross flow and longitudinal flow, on the heat dissipation characteristics of system is discussed, as shown in Fig. 3. As shown in Fig. 4, the comparison of the maximum and minimum temperature of system under the above two liquid cooling layouts is shown respectively. It can be seen that under the same liquid cooling layout, the maximum and minimum temperature increases along the direction of liquid flow. This is mainly due to the greater temperature difference between battery and liquid at the inlet. As the flow along outlet direction, the heat transfer temperature difference gradually decreases, resulting in a gradual reduction in the heat transfer. Fig. 5 shows the temperature distribution of the battery module under different liquid cooling layouts. When the liquid cooling layout adopts cross flow, the maximum and minimum temperature are 307.07 K and 301.75 K, respectively. And the maximum temperature difference is 5.32 K. When the liquid cooling layout is longitudinal flow, the maximum and minimum temperature are 306.42 K and 301.45 K, respectively. And the maximum temperature difference is 4.97 K. By comprehensive comparison, the longitudinal flow has better heat dissipation performance than cross flow. This is mainly because the longitudinal flow has a larger heat transfer area than cross flow. However, due to the consistency of flow direction at the liquid cooling inlet, it is easy to cause the battery module to still have a large temperature difference.

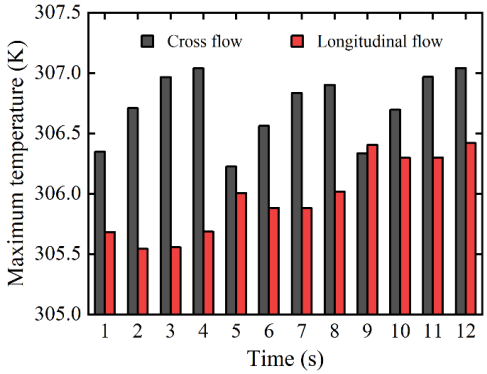

(a)

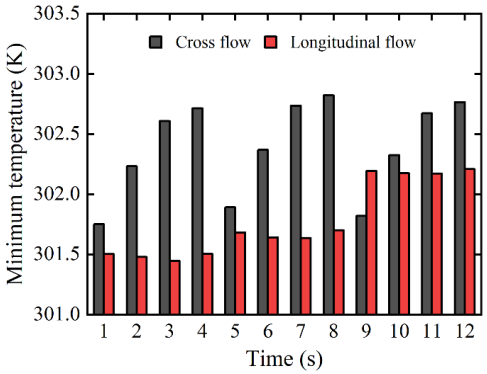

(b)

Fig. 4. Temperature contrast. (a) Maximum temperature; (b) Minimum temperature.

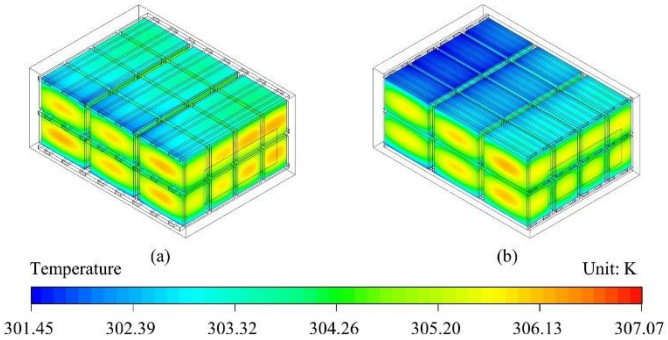

Fig. 5. Temperature distribution.

3.2 Effect of liquid cooling flow direction

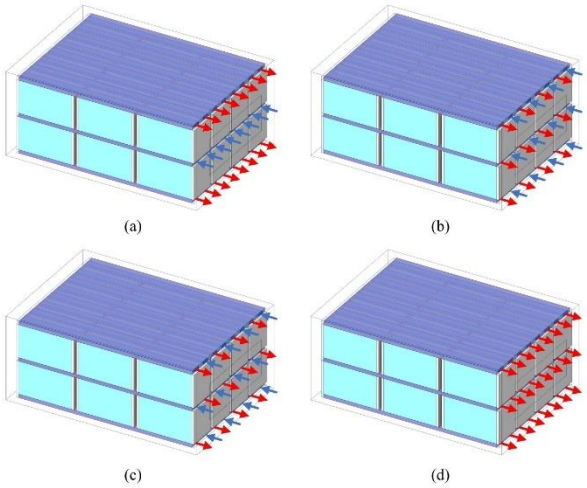

Fig. 6. Liquid cooling flow direction. (a) Case A; (b) Case B; (c) Case C; (d) Case D.

Further, in order to improve temperature uniformity of battery module, the flow direction of liquid cooling is improved, as shown in Fig. 6. Fig. 7 compares the temperature characteristics under four liquid cooling flow direction. Firstly, it can be seen from Fig. 7(a) that the maximum temperature is 306.09 K, 306.25 K, 306.12 K and 306.42 K respectively. Compared with case D, the maximum temperature of the other three flow schemes is reduced to a certain extent, which is reduced by 0.33 K, 0.17 K and 0.29 K respectively. Among them, the maximum temperature reduction effect of case A is the most significant. The maximum temperature difference of four flow schemes is 4.55 K, 4.48 K, 4.35 K and 4.97 K, respectively. Compared with case D, the temperature uniformity of system is the best when the case C is adopted, and the improvement effect reaches 12.47%.

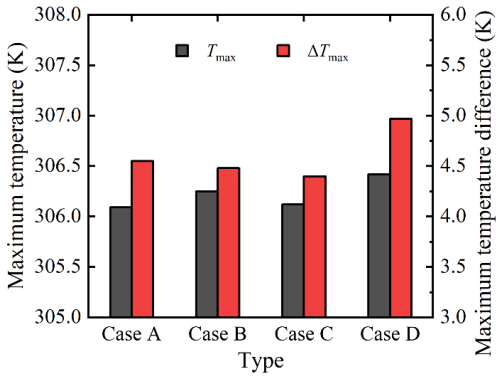

(a)

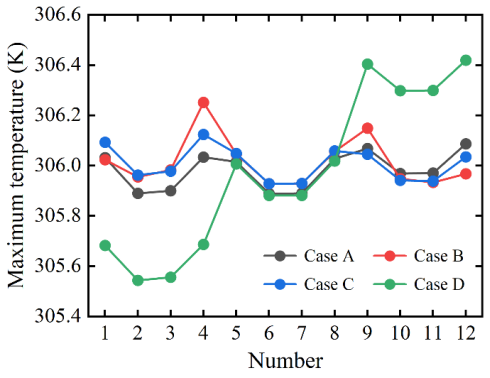

(b)

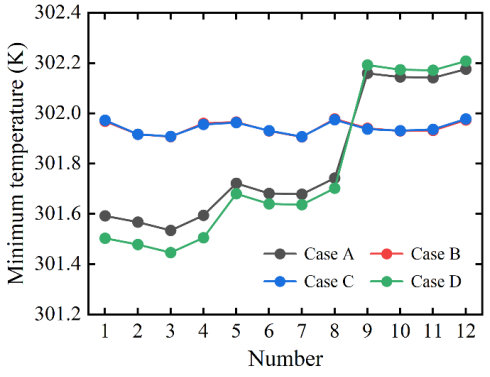

(c)

Fig. 7. Temperature characteristics analysis. (a) Temperature difference; (b) Maximum temperature; (c) Minimum temperature.

Figs. 7(b) and (c) show the maximum and minimum temperature comparison under four flow schemes. It can be seen that when any kind of counter flow scheme (Case A, Case B, Case C) is adopted, the maximum temperature and minimum temperature of No.1 - 4 battery pack have been increased to a certain extent. The maximum temperature and minimum temperature of No.9 - 12 battery pack have been decreased to a certain extent. On

the whole, the temperature difference between battery packs is smaller after the flow scheme is adopted.

3.3 Optimization design of cooling parameters

Table 3 Three factors and five levels of composite cooling.

Factors	Liquid (A)	Air (B)	Structure (C)
1	5	0	Type A
2	10	0.4	Type B
3	15	0.8	Type C
4	20	1.2	Type D
5	25	1.6	Type E

In order to further explore the interaction between air cooling and liquid cooling, this study takes the liquid cooling flow, air cooling velocity and flow structure as three factors of orthogonal test, which are represented by A, B and C respectively. Each factor is set to 5 levels, as shown in Table 3. The five structural types of composite flow are shown in Fig. 8. The liquid-cooled inlet temperature and the air-cooled inlet temperature are both 298.15 K, and the battery discharge rate is 2C. According to Table 2, the L25 (5^6) orthogonal table is selected, with a total of 25 orthogonal combinations. The maximum temperature and maximum temperature difference of battery module are used as orthogonal analysis indicators.

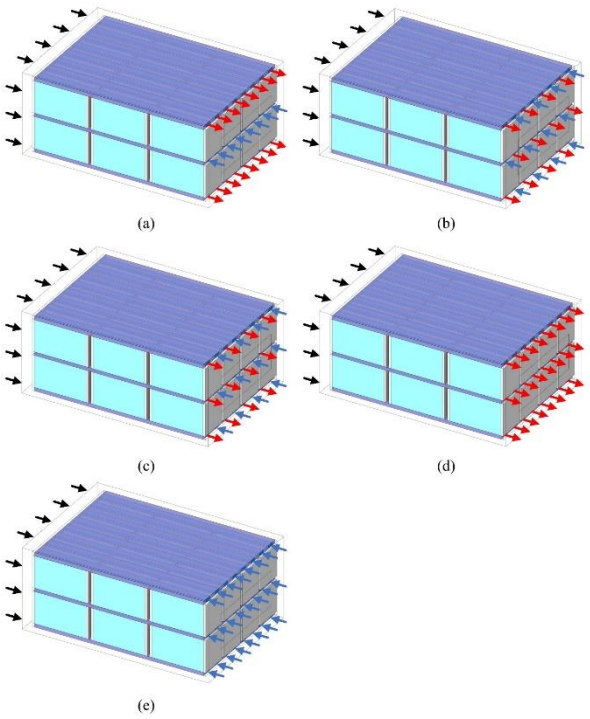

Fig. 8. Structural types of composite flow. (a) Type A; (b) Type B; (c) Type C; (d) Type D; (e) Type E.

Fig. 9(a) shows the relationship between maximum temperature and level of each factor. It can be seen that the maximum temperature change trend corresponding to each level of A factor is A1 > A2 > A3 > A4 > A5, which indicates that A5 level is the best value of A factor. Similarly, the levels of B5 and C2 are the best values of factor B and factor C, respectively. Therefore, the optimal parameter combination of the maximum temperature is A5B5C2.At this time, the liquid cooling flow rate is 25 L/min, the air-cooling flow rate is 1.6 m/s, and the composite flow structure type is Type B. Similarly, the optimal parameter combination for the maximum temperature difference is A4B2C2, as shown in Fig. 9(b). At this time, the liquid cooling flow rate is 20 L/min, the air-cooling velocity is 0.4 m/s, and the composite flow structure type is Type B.

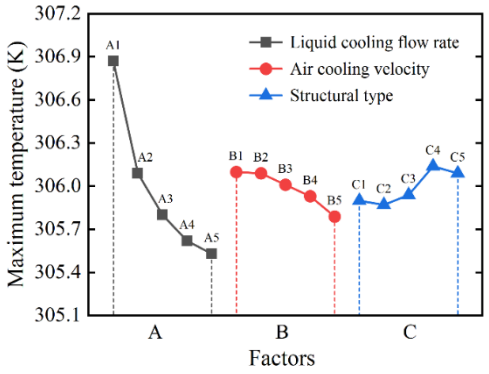

(a)

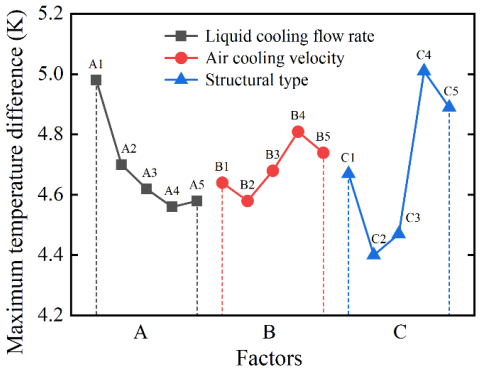

(b)

Fig. 9. The effect of factor level change on target performance. (a) Maximum temperature; (b) Maximum temperature difference.

Table 4 shows the thermal characteristics and power consumption of battery module under different optimization schemes. It can be seen that when the maximum temperature is the main optimization target, the maximum temperature and maximum temperature difference of battery module are 305.29 K and 4.43 K, respectively. When the maximum temperature difference is the main optimization objective, the maximum temperature and maximum temperature difference are 305.60 K and 4.13 K, respectively. The maximum temperature of A4B2C2 scheme is only 0.31 K higher than that of the A5B5C2 scheme. However, the air-cooled pressure drop and liquid-cooled pressure drop of the latter system are reduced by 81.59% and 17.68% respectively compared with the former.

Therefore, considering the thermal characteristics and power consumption, the A4B2C2 optimization scheme can be selected as the cooling parameters at high discharge rate.

Table 4 Temperature characteristics and power consumption analysis of battery module.

Scheme	T_{max} (K)	T_{min} (K)	P_{air} (Pa)	P_{liquid} (Pa)
A5B5C2	305.29	4.43	241.2	81.68
A4B2C2	305.60	4.13	44.41	67.24

4. CONCLUSION

A novel composite cooling structure is proposed for high discharge rate scenarios. The cooling parameters are optimized based on the orthogonal analysis method. The conclusions are as follows. The system using liquid-cooled longitudinal flow has a better uniform temperature distribution than cross flow. The maximum temperature and maximum temperature difference of battery module are 306.42 K and 4.97 K, respectively. When the liquid cooling is completely counter flow, the maximum temperature difference is further reduced to 4.35 K, and the improvement effect is 12.47%. Further auxiliary air-cooling system, the maximum temperature difference is reduced to 4.13 K. The liquid cooling flow rate is 20 L/min, the air-cooling velocity is 0.4 m/s, and the composite flow structure type is Type B.

ACKNOWLEDGEMENT

This work was supported by the National Natural Science Foundation of China (No. 52206271) and the National Natural Science Foundation of China (No.52306266).

REFERENCE

[1] Conzen J, Lakshmipathy S, Kapahi A, Kraft S, DiDomizio M. Lithium ion battery energy storage systems (BESS) hazards, Journal of Loss Prevention in the Process Industries, 81 (2023) 104932.

[2] Chen D, Jiang J, Kim G-H, Yang C, Pesaran A. Comparison of different cooling methods for lithium ion battery cells, Applied Thermal Engineering, 94 (2016) 846-854.

[3] Ouyang D, Weng J, Chen M, Wang J. Impact of high-temperature environment on the optimal cycle rate of lithium-ion battery, Journal of Energy Storage, 28 (2020) 101242.

[4] Lan X, Li X, Ji S, Gao C, He Z. Design and optimization of a novel reverse layered air-cooling battery management system using U and Z type flow patterns, International Journal of Energy Research, 46 (2022) 14206-14226.

[5] Li M, Ma S, Jin H, Wang R, Jiang Y. Performance analysis of liquid cooling battery thermal management system in different cooling cases, Journal of Energy Storage, 72 (2023) 108651.

[6] Lin X-W, Zhou Z-F, Liu T-F, Xue S-Q, Liang Y, Zhang L-F, Liu B. Rate capability and Ragone plots for designing battery thermal management system based on phase change material, Journal of Energy Storage, 74 (2023) 109539.

[7] Weragoda DM, Tian G, Burkitbayev A, Lo K-H, Zhang T. A comprehensive review on heat pipe based battery thermal management systems, Applied Thermal Engineering, 224 (2023) 120070.

[8] Chen K, Zhang Z, Wu B, Song M, Wu X. An air-cooled system with a control strategy for efficient battery thermal management, Applied Thermal Engineering, 236 (2024) 121578.

[9] Zhang F, Lin A, Wang P, Liu P. Optimization design of a parallel air-cooled battery thermal management system with spoilers, Applied Thermal Engineering, 182 (2021) 116062.

[10] Fan Y, Wang Z, Fu T. Multi-objective optimization design of lithium-ion battery liquid cooling plate with double-layered dendritic channels, Applied Thermal Engineering, 199 (2021) 117541.

[11] Zuo W, Zhang Y, E J, Li J, Li Q, Zhang G. Performance comparison between single S-channel and double S-channel cold plate for thermal management of a prismatic LiFePO4 battery, Renewable Energy, 192 (2022) 46-57.

[12] Xin Q, Yang T, Zhang H, Yang J, Zeng J, Xiao J. Experimental and numerical study of lithium-ion battery thermal management system using composite phase change material and liquid cooling, Journal of Energy Storage, 71 (2023) 108003.